PCCP

PAPER

View Article Online
View Journal | View Issue

Cite this: *Phys. Chem. Chem. Phys.*, 2016, **18**, 22661

Received 19th May 2016,
Accepted 20th July 2016

DOI: 10.1039/c6cp03419e

www.rsc.org/pccp

Size-dependent concentrations of thermal vacancies in solid films†

Panpan Gao,[a] Quan Wu,[a] Xi Li,[a] Hongxin Ma,[a] Hao Zhang,[b] Alex A. Volinsky,[c] Lijie Qiao[a] and Yanjing Su*[a]

Solid films are considered as typical model systems to study size effects on thermal vacancy concentration in nanomaterials. By combining the generalized Young–Laplace equation with the chemical potential of vacancies, a strict size-dependent thermodynamic model of vacancies, which includes the surface intrinsic elastic parameters of the eigenstress, Young's modulus and the geometric size of the solid films, was established. The vacancy concentration changes in the film with respect to the bulk value, depending on the geometric size and surface stress sign of the solid films. Atomistic simulations of Au and Pt films verified the developed thermodynamic model. These results provide physical insights into the size-dependent thermal vacancy concentration in nanomaterials.

1. Introduction

Nanostructured materials possess many unique properties that differ from their bulk counterparts due to their high surface-to-volume ratio, size-dependent surface energy/stress, and possible quantum effects at the small scale. One of their unique properties is that the vacancy concentration changes significantly with the material size, especially at the nanometer scale.[1–3] Thermal vacancies play an important role in mechanical, optical, electrical and thermal properties.[4–9] A better knowledge of the role of the thermal vacancies in nanomaterials is vital for understanding their properties, behavior and application research in the future.

For sufficiently large systems, the concentration of thermal vacancies at a given temperature T and pressure P follows the Arrhenius empirical equation:

$$X_{\mathrm{v}} = \exp\left(-\frac{\mu_{\mathrm{v}}(T,P)}{k_{\mathrm{B}}T}\right), \tag{1}$$

where $\mu_{\mathrm{v}}(T, P) = \Delta H_{\mathrm{v}} - T\Delta S_{\mathrm{v}} + P\Delta V_{\mathrm{v}}$ is the chemical potential of vacancies, in which ΔH_{v} is the vacancy formation enthalpy at the standard state, ΔS_{v} is the formation entropy, ΔV_{v} is the formation volume, T is the absolute temperature and P is the hydrostatic pressure applied to the solid. Based on eqn (1), the applied stress will change the concentration of thermal vacancies in the solid by changing the chemical potential of the vacancies.

The surface stress and energy of solids have been studied for several decades by many researchers.[10–12] Surface stress will induce initial strain in the solid when its geometrical size decreases to the nanometer scale. Fresh surfaces without relaxation, created by cutting a crystal along the crystallographic plane, would have much higher surface energy. Energy minimization and relaxation of the separated freestanding crystals occur unavoidably, and atoms locally rearrange their positions to reduce the total energy.[13–15] The relaxation reduces the surface and total energies, but may lead to a change in the lattice spacing of a nanometer-sized material. Thus, it induces initial strain in the nanomaterial core.[16] Because of the initial deformation, both surface energy density and surface stress are size-dependent. It is reasonable to expect that the size-dependent surface stress of the nanomaterial will lead to the size-dependent concentration of thermal vacancies. To date, thermal vacancies have been quite difficult to study experimentally. However, positron annihilation is a well-established technique to study intrinsic defects in materials. For example, Mukherjee *et al.* carried out positron lifetime and Doppler broadening measurements of polymer-containing silver nanoparticles, and observed that the lifetime of the positrons trapped at the grain surface defects and the grain–polymer interface decreased with the grain size.[17] Nambissan *et al.* studied microstructure defects in $ZnFe_2O_4$ nanocrystals of various sizes, down to 5 nm, by positron lifetime measurements, and observed normal to inverse spinel transformation with size reduction.[18] Chaudhuri *et al.* described size-induced changes due to the defects in chemically synthesized ZnO nanoparticles.[19] The presence of zinc vacancies and charged oxygen vacancies

---

[a] *Corrosion and Protection Center, Key Laboratory for Environmental Fracture (MOE), University of Science and Technology Beijing, Beijing 100083, China. E-mail: yjsu@ustb.edu.cn*

[b] *Department of Chemical and Materials Engineering, University of Alberta, Edmonton, T6G 2 V4, Canada*

[c] *Department of Mechanical Engineering, University of South Florida, Tampa FL 33620, USA*

† Electronic supplementary information (ESI) available. See DOI: 10.1039/c6cp03419e

was demonstrated. The size-induced changes showed contrasting trends as the system size varied from 4 nm to 85 nm, and the critical size was 23 nm. Gao *et al.* investigated the evolution of vacancies in nanoporous Au(Pt) using positron annihilation spectroscopy and showed that there was a large vacancy concentration increase in the dealloying process.[20]

Many researchers have attempted to theoretically investigate the size-dependent vacancy formation energy in nanomaterials to understand the underlying physical mechanisms. Since the vacancy formation process involves breaking atomic bonds, it was thought that the vacancy formation energy could be related to the crystal cohesive energy based on the semi-empirical model.[21–23] Qi and Wang provided the relationship between the vacancy formation energy and the cohesive energy of small particles to conclude that the vacancy formation energy is lower than in the corresponding bulk metal.[24–27] Ouyang *et al.* presented an analytical model to address the vacancy formation energy in metallic nanoparticles under high temperature and pressure, based on the size-dependent cohesive energy consideration.[28–30] They found that the vacancy formation energy increases with particle size and that the vacancy formation energy on the surface and at the interface is smaller than in the interior core. Gladkikh *et al.* demonstrated that the cohesive energy and melting temperature display similar dependence on the particle size by calculating the size-dependent vacancy formation energy of nanomaterials using a proportionality between the vacancy formation energy and the melting temperature $E_\mathrm{v} = \vartheta T_\mathrm{m}$.[31] Because the melting temperature, T_m, of small particles increases with particle size,[32] they concluded that the vacancy formation energy is lower in smaller particles. Guisbiers *et al.* developed a universal equation to describe the size and shape effects on many material properties. They developed a theoretical model to account for the size-dependent vacancy formation energy and entropy, based on the universal equation, and found that the vacancy concentration increases with decreasing sample size and increasing temperature.[33,34] However, Müller *et al.* reported an opposite result that the surface energy and surface stress contributions in metallic nanoparticles can actually increase the vacancy formation energy with decreasing particle size.[2] They also reported a decreased vacancy concentration with decreasing particle size. Recently Salis *et al.*[3] indicated that the total core and surface fractional concentrations had maxima at a certain particle radius because the surface energy increases both the core and surface vacancy formation energies, while the surface-to-volume ratio increases the relative concentration of surface defects with decreasing particle size.

In the present work, the solid film is considered as a typical model system to study the size-dependent concentration of thermal vacancies in nanomaterials. By analyzing the size-dependent surface stress of the solid films and the contribution of surface stress to the chemical potential of vacancies, an eigen size-dependent thermodynamic model of vacancies in solid films, which includes the surface eigenstress, Young's moduli of the surfaces and the core, the vacancy formation volume, and the geometric size of the solid films, was established. Molecular dynamics (MD) simulations with the embedded atom method (EAM) potentials of Au and Pt(001) solid films were used to verify the developed thermodynamic model. The effects of intrinsic surface elastic parameters, including the surface eigenstress and surface Young's modulus, on the size-dependent vacancy concentration in solid films are discussed, along with physical insights into the size-dependent thermal vacancy concentration in solid films.

2. Theoretical analysis

2.1 Size-dependent vacancy concentration

To understand the size-dependent vacancy concentration in nanomaterials, it is helpful to start from the definition of the vacancy formation energy in bulk materials.[2] The process of vacancy creation in a crystalline solid of N atoms consists of removing an atom from the volume of the crystal and inserting it into a reservoir with a certain chemical potential, μ_s. Denoting the cohesive energy per atom in the volume of the crystal as E_0, the energy of the perfect crystal is given by NE_0. The energy of the crystal with one atom removed is given by $(N-1)E_0 + \chi_0$, where χ_0 is the excess energy of the vacancy. Accordingly, the vacancy formation energy, E_v, is expressed as

$$E_\mathrm{v} = (N-1)E_0 + \chi_0 + \mu_\mathrm{s} - NE_0. \tag{2}$$

The thermal vacancy, also named the Schottky defect, can be created by removing one of the interior atoms from the crystal and replacing it with an atom on the crystal surface. In practice, when a Schottky defect is created, the crystal surface acts as the reservoir for the removed atom, and μ_s is the chemical potential of the crystal surface. One cautionary note is that μ_s is equal to the cohesive energy of the surface atoms E_s. Therefore, the vacancy formation energy in a bulk crystal can be written as

$$E_\mathrm{v} = (N-1)E_0 + \chi_0 + \mu_\mathrm{s} - NE_0 = \chi_0 + E_\mathrm{s} - E_0. \tag{3}$$

When a nanomaterial is created by removing it from a bulk material, relaxation occurs inevitably because of the high energy of the newly created surfaces. After relaxation, the surface stress causes initial strain in the core of the nanomaterial with respect to its bulk counterpart.[36,37] Consequently, the cohesive energy of the core atoms in the nanomaterial is given by $E_0^\mathrm{c} = E_0 + E_\mathrm{strain}^\mathrm{c}$, where $E_\mathrm{strain}^\mathrm{c}$ is the strain energy induced by the initial strain. The cohesive energy of the nanomaterial surface atoms is given by $E_\mathrm{s}^\mathrm{n} = E_\mathrm{s} + E_\mathrm{strain}^\mathrm{s}$, where $E_\mathrm{strain}^\mathrm{s}$ is the strain energy of the surface induced by the surface stress. It should be noted here that the surface of the bulk material is taken as the reference state. The excess energy of the vacancy in the core of the nanomaterial is given by $\chi_\mathrm{s}^\mathrm{n} = \chi_0 + \chi_\mathrm{strain}^\mathrm{c}$, where $\chi_\mathrm{strain}^\mathrm{c}$ is the change in the excess energy induced by the initial strain. The vacancy formation energy in the nanomaterial can be written as

$$E_\mathrm{v}^\mathrm{n} = (\chi_0 + E_\mathrm{s} - E_0) + (\chi_\mathrm{strain}^\mathrm{c} + E_\mathrm{strain}^\mathrm{s} - E_\mathrm{strain}^\mathrm{c}). \tag{4}$$

The initial deformation in the core and the surface stress of the nanomaterial are size-dependent, inducing size-dependent $\chi_\mathrm{strain}^\mathrm{c}$, $E_\mathrm{strain}^\mathrm{s}$ and $E_\mathrm{strain}^\mathrm{c}$. Consequently, the cohesive energy of the core atom, E_0^c, the cohesive energy of the surface atom,

E_s^n, and the excess energy of the vacancy, χ_s^n, are also size-dependent, resulting in size-dependent vacancy formation energy and equilibrium vacancy concentration in the nanomaterial.

2.2 Surface stress and initial strain in solid films

The present study focuses on the fundamental elastic properties of solid surfaces and thus considers solid films as typical structures to simplify the theoretical analysis. When a solid film is taken from its stress-free bulk counterpart, the film will relax to reach equilibrium and meet the energy minimization requirement due to the creation of a new surface. The relaxation process can be separated into normal relaxation and parallel relaxation.[36,37] After normal relaxation, an eigenstress σ_s^0 exists in the two-dimensional (2D) film surface, which is equal to the surface stress of the bulk material. After parallel relaxation, a stress (or initial strain ε^{ini}) will be generated in the three-dimensional (3D) core to balance the surface stress, and the 2D surfaces must undergo the same deformation as the core because the surfaces coherently adhere to the core, changing the surface stress to σ_s^{ini}.

If the normal state after relaxation is taken as the reference configuration state, the total potential energy of a film is given by

$$U(\varepsilon) = Su_s(\varepsilon) + Vu_c(\varepsilon), \tag{5}$$

where ε denotes strain, u_s is the generalized surface energy density per unit area, u_c is the core energy density per unit volume, and S and V are the surface area and volume of the film, respectively.

For a solid film with thickness h and length L_0 after relaxation, the energy density is given by

$$u_s(\varepsilon) = u_s^0 + 2\times(\sigma_s^0\varepsilon) + 2\times\left(\frac{1}{2}Y_s\varepsilon^2\right) \tag{6a}$$

$$u_c(\varepsilon) = u_c^0 + 2\times\left(\frac{1}{2}Y_c\varepsilon^2\right), \tag{6b}$$

where u_s^0 and u_c^0 are the generalized surface and core energy densities in the strain-free state, respectively; σ_s^0 is the biaxial surface eigenstress in the 2D surface; and Y_c and Y_s are the biaxial Young's moduli of the core and surface, respectively. Substituting eqn (6a) and (6b) into eqn (5), the total potential energy of a solid film is given by

$$U(\varepsilon) = 2L_0^2(u_s^0 + 2\sigma_s^0\varepsilon + Y_s\varepsilon^2) + hL_0^2(u_c^0 + Y_c\varepsilon^2). \tag{7}$$

At equilibrium, the minimum energy requires $\partial U(\varepsilon)/\partial\varepsilon|_{\varepsilon=\varepsilon^{ini}} = 0$, which yields the generalized Young–Laplace equation[35] to describe the mechanical force balance between the film surface and the core

$$2\sigma_s^0 + 2Y_s\varepsilon^{ini} + hY_c\varepsilon^{ini} = 0. \tag{8}$$

From eqn (8), the initial strain in the core induced by the surface stress is given by

$$\varepsilon^{ini} = -\frac{2\sigma_s^0}{2Y_s + hY_c}. \tag{9}$$

The biaxial surface and lattice stress of the solid film are then, respectively, given by

$$\sigma_s = \sigma_s^0 + Y_s\varepsilon^{ini} = \sigma_s^0\left(1 - \frac{2Y_s}{2Y_s + hY_c}\right) \tag{10}$$

$$\sigma_c = Y_c\varepsilon^{ini} = -\frac{2\sigma_s^0 Y_c}{2Y_s + hY_c}. \tag{11}$$

2.3 Equilibrium vacancy concentration in solid films

For sufficiently large systems ($N > 10^3$ atoms), which consist of N atoms and n vacancies, the chemical potential of the vacancies is determined as follows:

$$\mu_v = \frac{\partial\Delta G}{\partial n} = \Delta H_v - T\Delta S_v^f + k_BT\ln\frac{n}{N+n}, \tag{12}$$

where k_B is the Boltzmann's constant and ΔS_v^f is the vibration entropy.

The standard chemical potential of the vacancies, μ_v^0, is determined as the change in the free energy of an infinite crystal per added vacancy, disregarding the mixing entropy,

$$\mu_v^0 = \Delta H_v - T\Delta S_v^f. \tag{13}$$

It is considered here that if n is a small quantity, the molar concentration of vacancies is given by

$$X_v \approx n/(N+n). \tag{14}$$

Consequently,

$$\mu_v = \mu_v^0 + k_BT\ln\frac{n}{N+n} = \mu_v^0 + k_BT\ln X_v. \tag{15}$$

The free energy of the crystal containing n vacancies can be represented in the form of a sum:

$$\Delta G = \sum_i N_i\mu_i + n\mu_v, \tag{16}$$

where N_i and μ_i are the number of atoms of type i and their chemical potential, respectively. Consequently, for the $\partial\Delta G/\partial n = 0$ equilibrium conditions at a given temperature, the number of vacancies, n, can be obtained from

$$\frac{\partial\Delta G}{\partial n} = \mu_v = \mu_v^0 + k_BT\ln X_v = 0. \tag{17}$$

From eqn (13), (15) and (17), the equilibrium concentration of the vacancies in a solid under the stress-free state is equal to

$$X_v^0 = \exp\left(-\frac{\mu_v^0}{k_BT}\right) = \exp\left(\frac{\Delta S_v}{k_B}\right)\exp\left(-\frac{\Delta H_v}{k_BT}\right). \tag{18}$$

The chemical potential of vacancies in a solid at constant temperature under applied hydrostatic pressure is given by

$$\tilde{\mu}_v = \mu_v^0 + k_BT\ln X_v + P\Delta V_v. \tag{19}$$

From eqn (19), the applied hydrostatic pressure alters the equilibrium vacancy concentration by changing the vacancy chemical potential. When normal stress components σ_{ii} (i = 1, 2, 3) are unequal, the hydrostatic stress[37–39] can be defined as $\sigma = \frac{1}{3}\sum_{i=1}^{3}\sigma_{ii}$. Thus, if we consider the biaxial lattice stress (σ_c) in the core of the solid film, the hydrostatic pressure P in eqn (19) can be replaced by $-2\sigma_c/3$. At equilibrium ($\tilde{\mu}_v = 0$), the concentration of vacancies in the core of the solid films is

$$\tilde{X}_v = X_v^0 \exp\left(\frac{2\sigma_c \Delta V_v}{3k_B T}\right), \tag{20}$$

where $X_v^0 = \exp\left(-\frac{\mu_v^0}{k_B T}\right)$ is the equilibrium concentration of the vacancies in the bulk of the stress-free solid. Substituting eqn (11) into eqn (20) yields

$$\tilde{X}_v = X_v^0 \exp\left[-\frac{4\sigma_s^0 Y_c \Delta V_v}{3(hY_c + 2Y_s)k_B T}\right]. \tag{21}$$

Eqn (21) is the eigen thermodynamic formulation of the equilibrium vacancy concentration in solid films. It shows that the vacancy concentration in solid films depends on the film thickness, the biaxial surface and bulk Young's moduli, the vacancy formation volume and the biaxial surface eigenstress for a given material at constant temperature.

When a vacancy is formed in a solid, it inevitably induces local tensile stress, contracting the lattice. The equilibrium vacancy concentration responds to the applied strain monotonically by decreasing (increasing) with compressive (tensile) strain. According to eqn (21), when the surface biaxial eigenstress is tensile ($\sigma_s^0 > 0$), the lattice stress in the film core is compressive, and the equilibrium vacancy concentration in the solid film is decreased compared with its bulk counterpart.

3. MD simulations of surface stress and vacancy formation energy in solid films

3.1 Bulk biaxial Young's modulus

MD simulations were conducted to extract the surface stress and initial strain in solid films. The MD simulations were performed using the LAMMPS code developed at the Sandia National Laboratories.[40] The MD simulations for the Au(001) and Pt(001) crystals were performed using the embedded-atom method (EAM) potentials.[41,42] The orthogonal coordinates of the x-, y-, and z-axes were set along the [100], [010], and [001] lattice directions, respectively, for all simulations, consistent with the theoretical analysis.

The simulations of bulk crystals were performed to obtain the reference energy, U_0, the equilibrium lattice constant and the bulk biaxial Young's modulus. To simulate the bulk material, a representative domain of 8 × 8 × 8 unit cells was adopted with periodical boundary conditions (PBCs) in all three directions. The reference energy and equilibrium lattice constant in the stress-free bulk crystals were obtained through energy minimization. The periodic lengths in all three directions were simultaneously adjusted, *i.e.*, the lattice constants were changed along the x-, y-, and z-directions. At a given periodic length, the system was relaxed to reach equilibrium and to obtain the total potential energy. The reference energy and equilibrium lattice constant were then determined at the minimum of the total potential energy at equilibrium. The bulk biaxial moduli were then determined from the simulations of biaxial compressive and tensile tests, which were conducted in two steps. (1) All atoms were displaced uniformly in the x–y plane, according to the uniform biaxial strain with 0.1% increment. (2) The plane stress conditions in the z-direction were identified by adjusting the periodic length along the z-direction to achieve the minimum total potential energy configuration. A strain range of −1% to 1% was adopted, corresponding to the initial strains in the film. Subsequently, energy density *versus* strain was fitted by using a quadratic function. The bulk biaxial Young's modulus was fitted from the second derivatives of the strain energy with respect to the applied strain ($\Delta U = U(\varepsilon) - U_0 = Y_c\varepsilon^2$).

3.2 The surface stress and initial strain in solid films

For solid film simulations, a film was created by placing atoms using the stress-free bulk lattice constant. PBCs were applied only in the x- and y-directions with free surfaces along the z-direction to emulate a representative element of an infinitely large film. The film thickness ranged from 2 nm to 50 nm, and the representative element had a size of 8 × 8 unit cells in the x- and y-directions. The relaxation of the films toward the minimum energy state was separated into two steps, *i.e.*, normal and parallel relaxations.[36,37] In normal relaxation, atoms were allowed to move in the z-direction to minimize the total energy with the prescribed representative film length L_0 in both x- and y-directions. After normal relaxation, parallel relaxation was conducted, in which atoms were allowed to move in all three directions. For a given number of unit cells, the total energy of the film depends on the film length L. When the parallel relaxation reaches the final equilibrium state, the energy is minimized, and the representative film length has its initial value L_{ini}. In simulations, the representative film length was changed, *i.e.*, the lattice constant was changed along both x- and y-directions. At a given representative length, the film was relaxed to obtain the total energy at equilibrium. The initial representative film length L_{ini} was then determined at the minimum of the total potential energy at equilibrium. Once the initial representative film length was determined, the initial strain ε^{ini} of the solid film was calculated as $\varepsilon^{\text{ini}} = \ln(L_{\text{ini}}/L_0)$.

3.3 The vacancy formation energy in solid films

It is assumed that a Schottky defect is created by extracting an atom from the solid film core and placing it on the film surface.[4] To determine the ideal bonding site, the adatom is moved on the crystal surface to find its position where the system potential energy is minimal.

The EAM potential was used to calculate the interactive forces between the atoms, along with the energy of the crystal. It is capable of simulating fcc metals with better accuracy and is ideal for calculating the vacancy formation energy. For the bulk material, the vacancy formation energy was calculated by taking the difference between the relaxation energy of removing an atom from the middle of the bulk crystal and the energy of the bulk crystal with the same number of atoms. The calculated vacancy formation energy of bulk Au and Pt is 1.03 eV and 1.68 eV, respectively, consistent with the reference.[26] After creation, the film was allowed to relax to the equilibrium state *via* energy minimization without any external constraints, calculating the total energy of the relaxed perfect crystal, U_T^p. An atom was extracted from the middle of the film, and then the adatom was placed on the surface, finding the minimized energy by relaxation, called the total energy, $U_\mathrm{T}^\mathrm{a-s}$. The calculation of the vacancy formation energy, E_v, has been previously simplified as the energy difference between the potential energy of the relaxed perfect crystal and the relaxed energy of adding an atom on the crystal surface. The vacancy formation energy can be calculated as

$$E_\mathrm{v} = U_\mathrm{T}^\mathrm{p} - U_\mathrm{T}^\mathrm{a-s}. \tag{22}$$

In the definition of the material vacancy concentration (eqn (18)), the term containing ΔS_v is relatively small and is disregarded here. The vacancy concentration of the solid film is then calculated as

$$X_\mathrm{v} = \exp\left(-\frac{E_\mathrm{v}}{k_\mathrm{B}T}\right). \tag{23}$$

4. Results and discussion

Fig. 1 shows the strain energy per unit volume, $U_\mathrm{c} - U_0$, plotted against the applied biaxial strain, ε_c, during loading and unloading under the traction-free conditions along the *z*-direction, indicating that the bulk Au and Pt crystals deform elastically within the applied strain range because the unloading data partially coincide with the loading data. Furthermore, the strain energy *versus* applied strain data could be fitted by a quadratic function, $U_\mathrm{c} - U_0 = Y_\mathrm{c}{\varepsilon_\mathrm{c}}^2$, as shown by the solid lines in Fig. 1, within the investigated strain range for the Au and Pt bulk crystals. In this case, Y_c is the bulk biaxial Young's modulus calculated from the second derivatives of the strain energy with respect to the applied strain, listed in Table 1. The bulk biaxial Young's moduli determined from the atomistic simulations will be utilized in the following analysis.

Eqn (8) can be rewritten as follows:

$$-hY_\mathrm{c}\varepsilon^\mathrm{ini} = 2\sigma_\mathrm{s}^0 + 2Y_\mathrm{s}\varepsilon^\mathrm{ini}, \tag{24}$$

where $F_\mathrm{c}^\mathrm{ini} = \sigma_\mathrm{c}^\mathrm{ini}h = hY_\mathrm{c}\varepsilon^\mathrm{ini}$ and $F_\mathrm{c}^\mathrm{ini} = \sigma_\mathrm{c}^\mathrm{ini} = \sigma_\mathrm{s}^0 + Y_\mathrm{s}\varepsilon^\mathrm{ini}$ denote the core force per unit length and surface force per unit length, respectively. Plotting $-F_\mathrm{c}^\mathrm{ini} = -hY_\mathrm{c}\varepsilon^\mathrm{ini}$ *versus* ε^ini yields a slope of $2Y_\mathrm{s}$ and an intercept of $2\sigma_\mathrm{s}^0$, meaning that the surface biaxial Young's modulus and eigenstress have been determined.

Fig. 2 shows the negative core force as a function of the core initial strain, where the solid lines are the fitting results, based on eqn (24). The surface eigenstress, σ_s^0, the biaxial Young's moduli, Y_s, and the core biaxial Young's moduli, Y_c, were extracted, as summarized in Table 1.

By substituting the data in Table 1 using eqn (10) and (11), one can obtain the surface stress σ_s and lattice stress σ_c in the core of solid films *versus* the film thickness, *h*. Fig. 3 shows the lattice stress and the surface stress of metal films *versus* thickness *h*. As expected, the lattice stress decreases exponentially

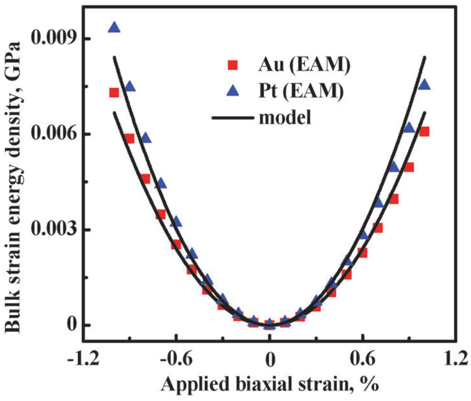

Fig. 1 Strain energy per unit volume as a function of the biaxial strain for the Au and Pt bulk crystals, where solid lines are fitting curves with the equation $U_\mathrm{c} - U_0 = Y_\mathrm{c}{\varepsilon_\mathrm{c}}^2$; biaxial strain loading is applied along the [100] and [010] directions, and the [001] direction is traction free.

Table 1 Lattice constant a_0, surface eigenstress σ_s^0, surface biaxial Young's moduli Y_s, bulk biaxial Young's moduli Y_c of Au(001) and Pt(001) solid films

Materials	a_0, Å	σ_s^0, N m^{-1}	Y_s, N m^{-1}	Y_c, GPa
Au(001)	4.08	1.56	14.27	66.81
Pt(001)	3.92	2.60	25.73	84.08

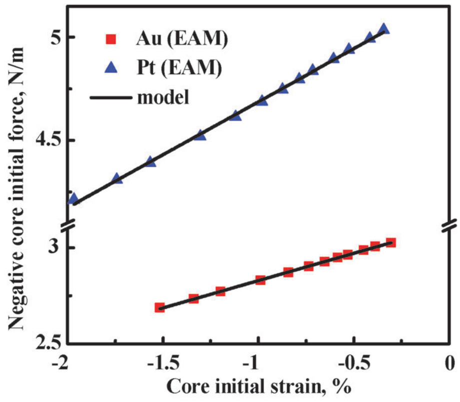

Fig. 2 Negative core force *versus* initial strain for the Au(001) films and the Pt(001) films. The solid lines are fitted using eqn (24).

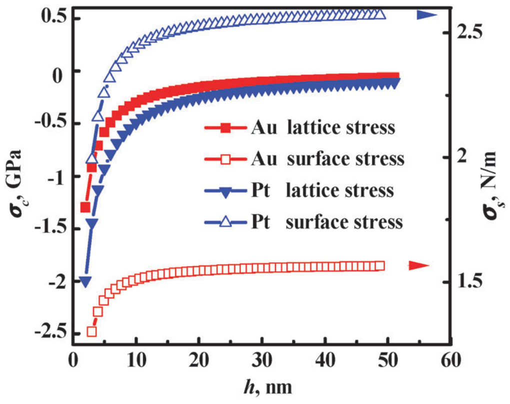

Fig. 3 The lattice stress and surface stress in solid film *vs.* film thickness *h*.

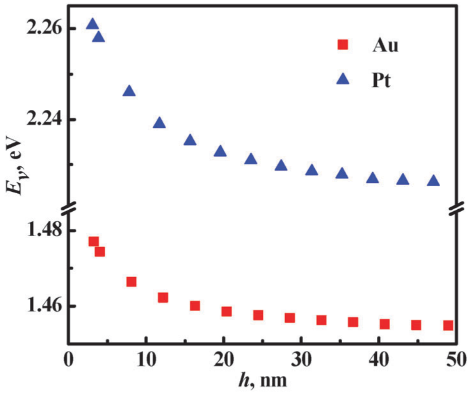

Fig. 4 MD simulation results of the vacancy formation energy *vs.* film thickness *h*.

with increasing film thickness. When the thickness is extremely large, the lattice stress decreases to zero. Obviously, the surface stress of the Au and Pt solid films exhibits a similar phenomenon, and the surface stress shows an exponential decrease when thickness *h* decreases to a few nanometers. For sufficiently thick films, the surface stress is almost the same as the surface eigenstress, which is equal to the surface stress of the bulk material. The Pt film exhibits larger variation than the Au film of both the surface stress and the lattice stress with the film thickness.

The vacancy formation energies obtained from MD simulations for different film thicknesses in Au and Pt with the (001) surface orientation at 0 K are plotted in Fig. 4. The MD data indicate that the vacancy formation energy increases exponentially with decreasing film thickness. The vacancy formation energy decreases smoothly until the bulk value is reached when the film thickness is sufficiently large.

Although the vacancy formation energy varies with temperature, there are very few changes at low temperature, which can be ignored in this study. We used the vacancy formation energy data obtained from MD simulations to calculate the vacancy concentrations from eqn (23) at room temperature T = 300 K. According to the cell parameters, the Au and Pt atomic volumes are 1.69×10^{-29} m^3 and 1.51×10^{-29} m^3, respectively. The formation volume for a vacancy in Au and Pt is equal to 0.52 and 0.7 times the atomic volume, respectively.[43,44] The surface and core elastic properties, along with the surface stress used for calculating the plots in Fig. 5, are listed in Table 1. The size-dependent vacancy concentration to bulk vacancy concentration ratio obtained from the MD simulation is plotted in Fig. 5, along with the predictions from eqn (21). The MD data show an obvious depletion of the vacancy concentration with decreasing film thickness, in quantitative agreement with eqn (21). Fig. 5 shows that the vacancy concentration in the film is greatly decreased compared with the bulk material when the film thickness decreases. This means that it is difficult to form vacancies in solid films.

It should be noted that the Au or Pt solid films exhibit a tensile surface stress, observed from the MD simulation results, which causes compressive lattice stress and also compressive strain in the core of the films. It is known that a certain concentration of vacancies causes volume expansion. If there is volume shrinkage, the vacancy concentration decreases correspondingly. Therefore, the equilibrium vacancy concentration decreases due to the tensile surface stress in Au and Pt solid films. Conversely, if there is compressive surface stress in the solid films, one can expect that it will cause an increase in vacancy concentration.

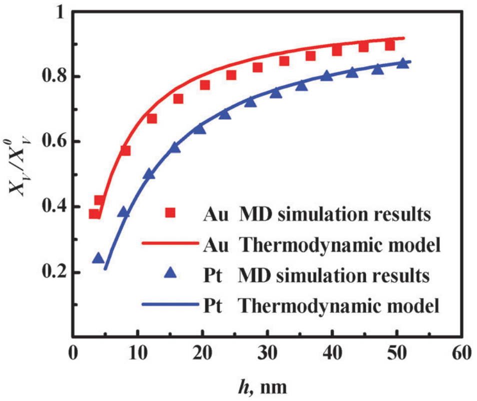

Fig. 5 MD simulation results and the theoretical calculations of the vacancy concentration in solid films to vacancy concentration in bulk materials ratio *vs.* the film thickness at room temperature T = 300 K.

5. Conclusions

In summary, by considering the surface energy and surface stress, an eigen thermodynamic model for the vacancies in solid films, which includes the intrinsic physical parameters, such as the surface eigenstress, surface and core Young's moduli, vacancy formation volume, and geometric size of the solid films, was established. The size-dependent surface stress of the nanomaterial leads to the size-dependent chemical potential of thermal vacancies and the size-dependent vacancy concentration. The model shows that the vacancy concentration decreases with decreasing material size. These results have been verified by the MD simulations of Au and Pt with the (001) surface orientation, taking into account the surface stress effects.

Acknowledgements

This work was supported by the National Basic Research Program of China (Grant No. 2012CB937502), Beijing government foundation (No. Z151100001615047) and the National Science Foundation (IRES 1358088).

References

1 G. Guisbiers, *J. Phys. Chem. C*, 2011, **115**, 2616.
2 M. Müller and K. Albe, *Acta Mater.*, 2007, **55**, 3237.
3 M. Salis, C. M. Carbonaro, M. Marceddu and P. C. Ricci, *Nanosci. Nanotechnol.*, 2013, **3**, 27.
4 Y. Kraftmakher, *Phys. Rep.*, 1998, **299**, 79.

5 D. C. Look, J. W. Hemsky and J. R. Sizelove, *Phys. Rev. Lett.*, 1999, **82**, 2552.

6 J. T. Yates Jr., *Surf. Sci.*, 2009, **603**, 1605.

7 G. Ouyang, C. X. Wang and G. W. Yang, *Chem. Rev.*, 2009, **109**, 4221.

8 H. B. Zeng, W. P. Cai, P. S. Liu, X. X. Xu, H. J. Zhou, C. Klingshirn and H. Kalt, *ACS Nano*, 2008, **2**, 1661.

9 S. B. Zhang, S. H. Wei and A. Zunger, *Phys. Rev. B: Condens. Matter Mater. Phys.*, 2001, **63**, 075205.

10 R. Shuttleworth, *Proc. Phys. Soc., London, Sect. A*, 1950, **63**, 444.

11 M. M. Nicolson, *Proc. R. Soc. A*, 1955, **228**, 490.

12 E. Orowan, *Proc. R. Soc. A*, 1970, **316**, 473.

13 J. Diao, K. Gall, M. L. Dunn and J. A. Zimmerman, *Acta Mater.*, 2006, **54**, 643.

14 H. Liang, M. Upmanyu and H. Huang, *Phys. Rev. B: Condens. Matter Mater. Phys.*, 2005, **71**, 241403.

15 W. J. Huang, R. Sun, J. Tao, L. D. Menard, R. G. Nuzzo and J. M. Zuo, *Nat. Mater.*, 2008, **7**, 308.

16 T. Y. Zhang, M. Luo and W. K. Chan, *J. Appl. Phys.*, 2008, **103**, 104308.

17 M. Mukherjee, D. Chakravorty and P. M. G. Nambissan, *Phys. Rev. B: Condens. Matter Mater. Phys.*, 1998, **57**, 848.

18 P. M. G. Nambissan, C. Upadhyay and H. C. Verma, *J. Appl. Phys.*, 2003, **93**, 6320.

19 S. K. Chaudhuri, M. Ghosh, D. Das and A. K. Raychaudhuri, *J. Appl. Phys.*, 2010, **108**, 064319.

20 P. P. Gao, Z. J. Zhu, X. L. Ye, Y. C. Wu, H. J. Jin, A. A. Volinsky, L. J. Qiao and Y. J. Su, *Scr. Mater.*, 2016, **113**, 68.

21 C. C. Yang and S. Li, *Phys. Rev. B: Condens. Matter Mater. Phys.*, 2007, **75**, 165413.

22 M. A. Shandiz, A. Safaei, S. Sanjabi and Z. H. Barber, *Solid State Commun.*, 2008, **145**, 432.

23 S. C. Vanithakumari and K. K. Nanda, *Phys. Lett. A*, 2008, **372**, 6930.

24 W. H. Qi and M. P. Wang, *Physica B*, 2003, **334**, 432.

25 W. H. Qi and M. P. Wang, *J. Mater. Sci.*, 2004, **39**, 2529.

26 W. H. Qi, M. P. Wang, M. Zhou and W. Y. Hu, *J. Phys. D: Appl. Phys.*, 2005, **38**, 1429.

27 D. Xie, M. P. Wang and L. F. Cao, *J. Mater. Sci.*, 2005, **40**, 3565.

28 G. Ouyang, W. G. Zhu, G. W. Yang and Z. M. Zhu, *J. Phys. Chem. C*, 2010, **114**, 4929.

29 G. Ouyang, W. G. Zhu, C. Q. Sun, Z. M. Zhu and S. Z. Liao, *Phys. Chem. Chem. Phys.*, 2010, **12**, 1543.

30 G. Ouyang, C. Q. Sun and W. G. Zhu, *J. Phys. Chem. C*, 2009, **113**, 9516.

31 N. T. Gladkikh and O. P. Kryshtal, *Funct. Mater.*, 1999, **6**, 823.

32 N. T. Gladkikh, A. P. Kryshtal and S. I. Bogatyrenko, *J. Tech. Phys.*, 2010, **55**, 1657.

33 G. Guisbiers and L. Buchaillot, *Phys. Lett. A*, 2009, **374**, 305.

34 G. Guisbiers, *Res. Lett.*, 2010, **5**, 1132.

35 T. Chen, M. S. Chiu and C. N. Weng, *J. Appl. Phys.*, 2006, **100**, 074308.

36 T. Y. Zhang, Z. J. Wang and W. K. Chan, *Phys. Rev. B: Condens. Matter Mater. Phys.*, 2010, **81**, 195427.

37 T. Y. Zhang and H. Ren, *Acta Mater.*, 2013, **61**, 477.

38 F. C. Larche and J. W. Cahn, *Acta Metall.*, 1985, **33**, 331.

39 J. W. Cahn and F. C. Larche, *Acta Metall.*, 1982, **30**, 51.

40 S. Plimpton, *J. Comput. Phys.*, 1995, **117**, 1.

41 M. S. Daw and M. I. Baskes, *Phys. Rev. B: Condens. Matter Mater. Phys.*, 1984, **29**, 6443.

42 S. M. Foiles, M. I. Baskes and M. S. Daw, *Phys. Rev. B: Condens. Matter Mater. Phys.*, 1986, **33**, 7983.

43 H. H. Grimes, *J. Phys. Chem. Solids*, 1965, **26**, 509.

44 R. M. Emrick and P. B. McArdle, *Phys. Rev. B: Solid State*, 1972, **6**, 1144.